

Optimum LoRaWAN Configuration Under Wi-SUN Interference

Arliones Hoeller Jr., Richard Demo Souza, Hirley Alves, Onel L. Alcaraz López, Samuel Montejo-Sánchez, Marcelo Eduardo Pellenz

Abstract—Smart Utility Networks (SUN) rely on the Wireless-SUN (Wi-SUN) specification for years. Recently, however, practitioners and researchers have also considered Low-Power Wide-Area Networks (LPWAN) like LoRaWAN for such applications. With distinct technologies deployed in the same area and sharing unlicensed bands, one can expect these networks to interfere with one another. This paper builds over a LoRaWAN model to optimize network parameters while accounting for the interference from other technologies. Our analytic model accounts for the interference LoRaWAN receives from IEEE 802.15.4G networks, which form the bottom layers of Wi-SUN systems. We also derive closed-form equations for the expected reliability of LoRaWAN in such scenarios. We set the model parameters with data from real measurements of the interplay among the technologies. Finally, we propose two optimization algorithms to determine the best LoRaWAN configuration given a targeted minimum reliability level as a restriction. The first algorithm maximizes communication range given a constraint on the minimum number of users, and the second maximizes the number of users given a minimum communication range. We validate the models and algorithms through numerical analysis and simulations. The proposed methods are useful tools for planning interference-limited networks with requirements of minimum reliability.

Keywords—Internet of Things, Long-Range Low-Power Communications, LoRaWAN, Communication Interference.

I. INTRODUCTION

Smart Utility Networks (SUN) have gained increased attention in recent years as key enablers of Smart Cities [1]. In such smart environments, the Internet-of-Things (IoT) will

play a paramount role in connecting a massive number of devices such as smart meters, smart light bulbs, and smart appliances. Besides the existence of several potential network technologies, e.g., LoRaWAN, SigFox, and Wi-SUN, the efficient connection of massive numbers of devices is still a challenge if the reliability requirements are high [2].

The industry has backed two significant initiatives: LORA ALLIANCE and WI-SUN ALLIANCE. The LORA ALLIANCE – supported by Semtech, IBM, Cisco, Orange, among others – maintains the LoRaWAN specification [3]. LoRaWAN is a Low-Power Wide Area Network (LPWAN) technology operating in the sub-GHz ISM band, using chirp spread-spectrum modulation, allowing increased signal robustness and range at low power consumption and low data rates [1]. LoRaWAN uses the LORA physical (PHY) layer designed by Semtech and specifies the upper layer protocols to enable IoT deployments. The WI-SUN ALLIANCE – supported by Cisco, Analog Devices, Toshiba, and others – maintains the Wi-SUN specification [4], [5]. Wi-SUN is a Field Area Network (FAN) technology built upon the physical and link layers defined by the IEEE 802.15.4G standard. IEEE 802.15.4G operates in different bands of the ISM, including the same sub-GHz bands used by LoRaWAN, where it uses a Gaussian Frequency Shift Keying (GFSK) modulation over narrow-band channels. Besides those bottom layers, Wi-SUN also defines network- and application-level services, including profiles for specific utility applications (e.g., energy, gas, water).

While utility service providers modernize their systems to use smart meters, deployments can use different communication technologies in the same geographical region, thus raising the question of how inter-technology interference affects network scalability. Coordination among transmissions in different technologies is unfeasible at the network or lower layers, so it is essential to understand the impact of these sources of interference. To achieve a realistic model, one should take into account that LPWAN devices in the ISM radio band are subject to interference generated by other networks sharing the same part of the spectrum. For instance, different authors report the analysis of the interaction of LORA with other technologies considering IEEE 802.15.4G [6], SigFox [7], [8] and IEEE 802.11AH [8]. The results in those papers suggest that LORA susceptibility to interference arriving from other technologies depends not only on the activity on those interfering networks but also on the configuration of the LORA signal, mainly the spreading factor (SF). In this paper, we consider LoRaWAN as our target technology and model its performance in the presence of IEEE 802.15.4G interference sources in the sub-

A. Hoeller-Jr. is with the Dept. of Telecommunications Engineering, Fed. Institute for Education, Science, and Technology of Santa Catarina, Brazil, arliones.hoeller@ifsc.edu.br.

R. D. Souza and A. Hoeller-Jr. are with the Dept. of Electrical and Electronics Engineering, Fed. Univ. of Santa Catarina, Brazil, richard.demo@ufsc.br.

H. Alves and O. L. A. López are with the Centre for Wireless Communications, Univ. of Oulu, Finland, {Onel.AlcarazLopez,Hirley.Alves}@oulu.fi.

S. Montejo-Sánchez is with Programa Institucional de Fomento a la I+D+i, Universidad Tecnológica Metropolitana, Chile, smontejo@utem.cl.

M. E. Pellenz is with the Pontifical Catholic University of Paraná, Brazil, marcelo@ppgia.pucpr.br.

This work has been partially supported in Brazil by CNPq and EdP Brazil through the R&D ANEEL Project (Grant PD-00380-0027/2018); in Finland by Academy of Finland (Aka) 6Genesis Flagship (Grant 318927), EE-IoT (Grant 319008) and Aka Prof (Grant 307492); and in Chile by FONDECYT Postdoctoral (Grant 3170021).

©2019 IEEE. Personal use of this material is permitted. Permission from IEEE must be obtained for all other uses, in any current or future media, including reprinting/republishing this material for advertising or promotional purposes, creating new collective works, for resale or redistribution to servers or lists, or reuse of any copyrighted component of this work in other works.

GHz ISM band (e.g., around 868 MHz in Europe and 915 MHz in USA/Brazil). Please note that the restriction of the model to IEEE 802.15.4G interference comes without loss of generality since one can extend it to other network technologies provided that appropriate isolation thresholds between the technologies are available.

While we focus on modeling how IEEE 802.15.4G affects LORAWAN, we evolve from previous developments in [9] and [10] to approach the problem from an analytic perspective. We use the proposed models to derive two optimization algorithms that allow for the exploration of the configuration space of LORAWAN in the presence of internal and external IEEE 802.15.4G interference. The proposed algorithms are tools for network planning, guiding the trading-off between the number of nodes and coverage area. We validate our analytic finds using simulations configured according to experimental results on the interplay between these networks published in [6].

The contributions of this work include a closed-form expression for the inter-SF LORAWAN interference analytic model of [10]; the extension of the analytic models of [9] and [10] to consider external interference; the performance analysis of LORAWAN considering the experimental results on inter-technology interference from [6]; and two novel algorithms to optimize LORAWAN configuration, either in terms of network load or communication range, under reliability constraints.

The remaining of this paper is organized as follows. Section II summarizes related work, and Section III briefly introduces the characteristics of LORAWAN and IEEE 802.15.4G. Section IV introduces the proposed system model and the outage models. Section V presents the proposed algorithms. Section VI evaluates the models and algorithms. Section VII concludes the paper.

II. RELATED WORK

Georgiou and Raza [11] propose an analytic model of LORAWAN which considers both disconnection and collision probabilities in Rayleigh fading channels. They show that LORAWAN is sensitive to node density because it affects collision probability. In [9], we extend the work of [11] to exploit message replications and multiple receive antennas at the gateway. We show that message replication is an interesting option for low-density networks, while the performance gains from spatial diversity are significant in all cases. Mahmood *et al.* [10], as well as we [9] and Georgiou and Raza [11], use stochastic geometry and Poisson Point Processes (PPP) to derive analytic models of the coverage probability of LORAWAN. Contrasting with [11] and [9], the work in [10] takes into account the effect of interference from the imperfect orthogonality of LORA signals using different SFs. In this sense, Croce *et al.* [12] show that LORA SF separation is not perfect, so LORA nodes are subject to some interference generated by nodes using other SFs.

Sørensen *et al.* [13] propose analytic models to investigate the performance of LORAWAN uplink regarding latency, collision, and throughput. They also explore the network resource allocation for given QoS requirements and traffic models.

Pop *et al.* [14] evaluate how LORAWAN downlink impacts uplink. They consider the medium access control (MAC) layer and, through simulations, verify that if too many end-devices request delivery confirmation, the downlink becomes unstable and unable to deliver several acknowledgment packets, thus forcing nodes to retry, ultimately flooding the network.

Orfanidis *et al.* [6] report an experimental evaluation of the interference between IEEE 802.15.4G and LORA by measuring the packet error ratio in different SINR scenarios inside an anechoic chamber. The measurements consider a single IEEE 802.15.4G interferer over one LORA link. Their results show that lower SFs are more susceptible to interference. Although these measurements show interesting results, it is important to note that they consider a limited number of nodes, thus making it hard to extrapolate the conclusions. To the best of our knowledge, no other work has studied the susceptibility of LORA to external IEEE 802.15.4G interference, and there is none published work that investigates this relationship in a network-scale scenario with several active links in both IEEE 802.15.4G and LORAWAN.

III. LPWAN NETWORKS

LPWANs employ low-power communication technologies that enable the connection of thousands of IoT devices. Most of these technologies work in frequencies below 1 GHz and employ modulation techniques that enable link budgets of 150 ± 10 dB, resulting in robust communication channels with low energy consumption reaching distances in the order of kilometers [1]. Additionally, for reducing complexity and energy consumption, LPWAN technologies use MAC protocols that may decrease the efficiency of channel use. For instance, both LORAWAN and SIGFOX transmit data using unslotted ALOHA, which is known to present high collision probability when a large number of stations are connected [15].

A. LORAWAN

LORA is a proprietary sub-GHz chirp spread spectrum modulation technique optimized for long-range applications and low power consumption at slow transmission rates [3]. LORA modulation depends, basically, on three parameters [16]: bandwidth (B), usually set to 125 kHz or 250 kHz for uplink and 500 kHz for downlink; SF, which assumes values from 7 up to 12; and the forward error correction (FEC) rate, varying from $\frac{4}{8}$ to $\frac{4}{5}$. From these parameters, one can extract the packet Time-on-Air (ToA), the receiver sensitivity, and the required signal to noise ratio (SNR) for successful detection in the absence of interference. Table I features the relation among LORA parameters, given a packet configuration, showing that ToA grows exponentially with SF, reducing the bit rate while increasing the receiver sensitivity, thus allowing higher coverage.

The implementation of LORA PHY is agnostic of higher layers. LORAWAN is the most widely used protocol stack for LORA networks. It implements a star topology where *end-devices* (nodes) connect through a single-hop to one or more *gateways*, which in turn connect to a *network server* via an IP network. LORAWAN MAC uses the unslotted ALOHA [15]. Moreover, a LORA gateway can process up to

Table I. LORA UPLINK CHARACTERISTICS CONSIDERING PACKETS OF 9 BYTES AT $B = 125$ KHZ WITH CRC AND HEADER MODE ENABLED, AND FEC RATE $\frac{4}{5}$ FOR THE SX1272 TRANSCEIVER [17].

SF i	ToA t_i (ms)	Bitrate Rb_i (kbps)	Receiver Sensitivity S_i (dBm)	SNR threshold ψ_i (dB)
7	41.22	5.47	-123	-6
8	72.19	3.12	-126	-9
9	144.38	1.76	-129	-12
10	247.81	0.98	-132	-15
11	495.62	0.54	-134.5	-17.5
12	991.23	0.29	-137	-20

nine channels in parallel, combining different sub-bands and SFs [1]. Besides, LORA features the capture effect, making it possible to recover a LORA signal when two or more signals are received simultaneously, in the same frequency and SF, provided that the desired signal is at least 1 dB above interference [12].

B. IEEE 802.15.4G

IEEE 802.15.4G is an amendment to the IEEE 802.15.4 standard focusing on Smart Utility Networks (SUN) that has been playing an important role in smart grid deployments [18]. The standard specifies different modes able to operate in different frequency bands, including the Sub-GHz ISM bands used by LORAWAN. Data rates range from 40 to 1000 kbps, depending on the modulation and bandwidth in use [19].

Multi-Rate FSK (MR-FSK), with 2-FSK or 4-FSK, is the predominant modulation version in SUN applications due to its communication range [20]. In this configuration, the transceiver combines FSK modulation with Frequency Hopping Spread Spectrum (FHSS) to increase robustness [19]. The data rate may vary from 2.4 to 200 kbps, depending on region and frequency band. The mandatory configuration for all regions is 2-FSK operating at 50kbps, which implies a channel spacing of 200 kHz. The receiver sensitivity for a PER of 10% must be better than -85 dBm or -91 dBm at, respectively, 200 and 50 kbps, without FEC. If FEC is enabled, the sensitivity must drop to -91 dBm and -97 dBm for the same data rates. Transmit power depends on regional regulations, but must be at least -3 dBm [5]. Most configurations use 14dBm transmit power and 1% duty cycle [21].

IEEE 802.15.4G proposes extensions to the MAC mechanisms defined by IEEE 802.15.4E amendment [22] and makes extensive use of low-energy modes. The IEEE 802.15.4G networks are expected to form multi-hop, mesh networks. Before sending data, the MAC layer performs either carrier sense or a simplified version of channel monitoring named Coordinated Sampled Listening (CSL) [23].

IV. SYSTEM MODEL

Following the developments in [9] and [10], we use a set of Poisson Point Processes (PPP) [24]. Our model considers nodes deployed uniformly in a circular region around a gateway. Figure 1 illustrates a possible setup where SF increases according to the distance from the gateway. The vector $L = [l_0, \dots, l_6]$, $l_0 = 0$, defines the limits of each SF ring.

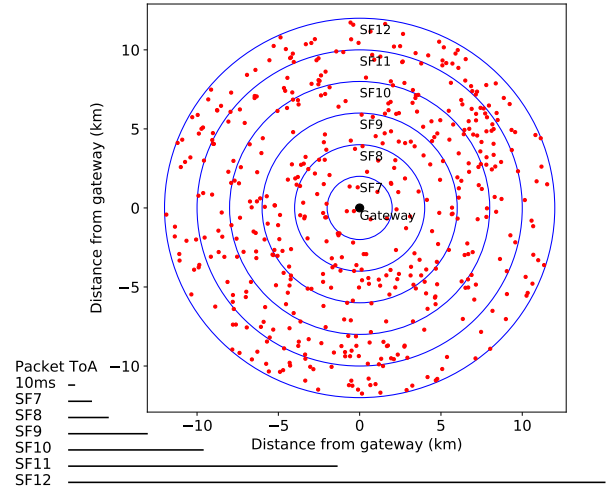


Figure 1. $\bar{N} = 500$ nodes uniformly distributed in a circular area of radius $R = 12000$ m around the gateway and with increasing SF every 2000 m. The ToA, as in Table I, is illustrated in the lower-left corner.

Note that $R = l_6$ is the maximum network communication range, *i.e.*, the coverage radius. LORAWAN devices transmit in the uplink at random using the ALOHA protocol and transmit once in a given period T . Considering that all nodes run the same application, the network usage is different for each SF because of different data rates (see ToA in Table I). Figure 1 also shows the ToA difference graphically. Hence, we model the transmission probability of LORAWAN devices as a vector $p = [p_1, \dots, p_6]$, $p_i \in (0, 1] \forall i \in \{1, \dots, 6\}$, and $p_i = \frac{t_i}{T}$, where t_i is the ToA for SF of ring i . Note that, for the sake of simplicity, we define the set $S = \{1, \dots, 6\}$ to denote the SF rings and that each ring uses a respective SF in $\{7, \dots, 12\}$.

Each LORAWAN SF ring constitutes a separated PPP, denoted Φ_i , $i \in S$, making it possible to attribute different densities to each SF. Φ_i has density $\alpha_i = p_i \rho_i$ in its area $V_i = \pi(l_i^2 - l_{i-1}^2)$, where l_{i-1} and l_i are, respectively, the inner and outer radii of SF ring i (from L), and ρ_i is the spatial density of nodes in V_i . Similarly, we model the IEEE 802.15.4G network as an additional PPP where nodes transmit with probability $p_z \in (0, 1]$. The PPP Φ_z has density $\alpha_z = p_z \rho_z$ in the area $V_z = \pi R_z^2$, where ρ_z is the spatial density of nodes in V_z . The average number of nodes in Φ_i is $\bar{N}_i = \rho_i V_i$, for LORAWAN, and $\bar{N}_z = \rho_z V_z$, for IEEE 802.15.4G. The average number of nodes in the LORAWAN network is $\bar{N} = \sum_{i \in S} \rho_i V_i$.

For instance, take the ring $i = 2$ in Figure 1, defined by two circles of radii $l_1 = 2$ km and $l_2 = 4$ km. Nodes in this ring use SF_8 . The ring area is $V_2 = \pi(l_2^2 - l_1^2) = 37.7$ km². If there are, on average, $\bar{N}_2 = V_2 \rho_2 = 100$ nodes in this ring, then its spatial density is $\rho_2 = \frac{\bar{N}_2}{V_2} = 2.65$ nodes/km². Finally, if nodes transmit probability is 1% ($p_2 = 0.01$), the density of Φ_2 is $\alpha_2 = p_2 \rho_2 = 0.0265$.

In our analysis, d_k is the Euclidean distance between the k -th node and the gateway, and d_1 denotes the distance of the node of interest. All nodes use the same transmit power \mathcal{P}_t to

send signal s_k , while both path loss and Rayleigh fading affect the received signals of LORAWAN and IEEE 802.15.4G. Path loss follows $g(d_k) = \left(\frac{\lambda}{4\pi d_k}\right)^\eta$, with wavelength λ , path loss exponent $\eta \geq 2$, while k represents a device in either network. Finally, h_k denotes the Rayleigh fading. Therefore, a LORAWAN signal r_1 received at the gateway is the sum of the attenuated transmitted signal s_1 , interference, and noise,

$$r_1 = g(d_1)h_1s_1 + \mathcal{I}_L + \mathcal{I}_Z + n, \quad (1)$$

where

$$\mathcal{I}_L = \sum_{i \in S} \sum_{k \in \Phi_i} g(d_k)h_k s_k, \quad (2)$$

accounts for intra-network interference, considering both co-SF and inter-SF interference by summing all other received signals from all SFs, and

$$\mathcal{I}_Z = \sum_{k \in \Phi_z} g(d_k)h_k s_k, \quad (3)$$

models external interference arising, in our case, from all active nodes in the IEEE 802.15.4G network. Finally, n is the additive white Gaussian noise (AWGN) with zero mean and variance $\mathcal{N} = -174 + F + 10\log_{10}(B)$ dBm, where $F = 6$ dB is the receiver noise figure and $B = 125$ kHz is the LORA channel bandwidth. The remainder of this section uses this model to derive the outage probability of LORAWAN links.

A. Outage Condition 1: Disconnection

Following [9], we consider the disconnection probability, which depends on the communication distance. A node is *not* connected to the gateway if the SNR of the received signal is below the threshold that allows successful detection in the absence of interference. Receiver sensitivity is different for each SF, what results in different SNR reception thresholds defined in

$$\Psi_{[dB]} = \begin{matrix} SF_7 & SF_8 & SF_9 & SF_{10} & SF_{11} & SF_{12} \\ [-6 & -9 & -12 & -15 & -17.5 & -20], \end{matrix}$$

where Ψ denotes the SNR threshold vector, and ψ_i denotes the i -th element of Ψ , *i.e.*, the SNR threshold for SF ring i . Then, we model the *connection probability* as

$$H_1(d_1) = \mathbb{P}[\text{SNR} \geq \psi_i | d_1]. \quad (4)$$

Since we assume Rayleigh fading, the instantaneous SNR is exponentially distributed [25], and therefore

$$H_1(d_1) = \mathbb{P}\left[\frac{\mathcal{P}_t |h_1|^2 g(d_1)}{\mathcal{N}} \geq \psi_i\right] = \exp\left(-\frac{\mathcal{N}\psi_i}{\mathcal{P}_t g(d_1)}\right). \quad (5)$$

B. Outage Condition 2: Intra-Network Interference

Intra-network interference arises from the activity of other devices in the same network. We follow [10] to model both co-SF and inter-SF interference. To recover a packet, the signal-to-interference ratio (SIR) at the gateway must be above a given threshold. The transceiver manufacturer informs that SFs are

orthogonal and that the co-SF SIR threshold is +6dB [17]. Goursaud *et al.* [26] propose theoretical SIR thresholds that match Semtech co-SF value but show that different SFs are not completely orthogonal. However, Croce *et al.* [12] showed, experimentally, that the SIR thresholds for Semtech SX1272 LORA transceiver are lower with regards to co-SF interference ($\approx +1$ dB) but significantly higher with respect to (w.r.t.) inter-SF interference. In this paper, we assume the experimental SIR thresholds of [12]

$$\Delta_{[dB]} = \begin{matrix} & SF_7 & SF_8 & SF_9 & SF_{10} & SF_{11} & SF_{12} \\ SF_7 & +1 & -8 & -9 & -9 & -9 & -9 \\ SF_8 & -11 & +1 & -11 & -12 & -13 & -13 \\ SF_9 & -15 & -13 & +1 & -13 & -14 & -15 \\ SF_{10} & -19 & -18 & -17 & +1 & -17 & -18 \\ SF_{11} & -22 & -22 & -21 & -20 & +1 & -20 \\ SF_{12} & -25 & -25 & -25 & -24 & -23 & +1 \end{matrix},$$

where Δ is the SIR threshold matrix, and $\delta_{i,j}$ denotes the element of Δ at the i -th line and j -th column, *i.e.*, the SIR threshold for the desired signal using SF $_i$ and interference using SF $_j$. Note that $i = j$ relates to the co-SF SIR while $i \neq j$ relates to inter-SF SIR. If one takes the SF $_7$ column as an example, it shows how SF $_7$ interference affects the LORA signals. Desired signals using higher SF are more robust to inter-SF interference, allowing for the decoding of LORA packets even if the interference power is much higher than the signal (*e.g.*, 25dB higher if the signal uses SF $_{12}$).

Following this rationale, we first use the formulations in [10] to analyze the success probability considering the interference from only one different SF $_j$. Let

$$\text{SIR}_j = \frac{|h_1|^2 g(d_1) \mathcal{P}_t}{\mathcal{I}_j}, \quad (6)$$

where the interference received from nodes using SF $_j$ is

$$\mathcal{I}_j = \sum_{k \in \Phi_j} |h_k|^2 g(d_k) \mathcal{P}_t. \quad (7)$$

Since the desired node at d_1 uses SF $_i$, the success probability is

$$\begin{aligned} P_{\text{SIR}_j}(d_1, j) &= \mathbb{P}[\text{SIR}_j \geq \delta_{i,j}] \\ &= \mathbb{E}_{\mathcal{I}_j} \left[\mathbb{P} \left[|h_1|^2 \geq \frac{\mathcal{I}_j \delta_{i,j}}{g(d_1) \mathcal{P}_t} \right] \right]. \end{aligned}$$

Since $|h_1|^2 \sim \exp(1)$,

$$P_{\text{SIR}_j}(d_1, j) = \mathbb{E}_{\mathcal{I}_j} \left[\exp \left(-\frac{\mathcal{I}_j \delta_{i,j}}{g(d_1) \mathcal{P}_t} \right) \right]. \quad (8)$$

Note that (8) has the form of the Laplace Transform w.r.t. \mathcal{I}_j , where $\mathcal{L}_{\mathcal{I}_j}(s) = \mathbb{E}_{\mathcal{I}_j}[\exp(-s\mathcal{I}_j)]$, $s = \frac{\delta_{i,j}}{g(d_1) \mathcal{P}_t}$. Thus, using (7) and applying the property of the sum of exponents,

$$P_{\text{SIR}_j}(d_1, j) = \mathbb{E}_{\Phi_j, |h_k|^2} \left[\prod_{k \in \Phi_j} \exp(-s |h_k|^2 g(d_k) \mathcal{P}_t) \right].$$

Solving the expectation over $|h_k|^2 \sim \exp(1)$ yields

$$P_{\text{SIR}_j}(d_1, j) = \mathbb{E}_{\Phi_j} \left[\prod_{k \in \Phi_j} \frac{1}{1 + sg(d_k) \mathcal{P}_t} \right].$$

Finally, we solve the expectation over the PPP Φ_j using the probability generating functional of the product over PPPs where $\mathbb{E}[\prod_{x \in \Phi_j} f(x)] = \exp[-\alpha_j \int_{\mathbb{R}^2} (1 - f(x)) dx]$, with α_j as the density of Φ_j , converting d_k to polar coordinates, and replacing s , obtaining

$$P_{\text{SIR}_j}(d_1, j) = \exp \left(-2\pi\alpha_j \int_{l_{j-1}}^{l_j} \frac{\delta_{i,j} d_1^\eta}{x^\eta + \delta_{i,j} d_1^\eta} x \, dx \right) \quad (9)$$

As a contribution over [10], we solve the integral in (9), called $f(\cdot)$ here. Assuming a generic SIR threshold γ , if we rearrange $f(\cdot)$ and evaluate the indefinite integral to apply the binomial theorem $(x+1)^{-1} = \sum_{k=0}^{\infty} (-1)^k x^k$ we have

$$\begin{aligned} f(d_1, \gamma, l_a, l_b) &= \int x \left(\frac{x^\eta}{d_1^\eta \gamma} + 1 \right)^{-1} dx \\ &= \int \sum_{k=0}^{\infty} \left(\frac{-1}{d_1^\eta \gamma} \right)^k x^{\eta k + 1} dx. \end{aligned}$$

Since $f(\cdot)$ is continuous in $\mathbb{R} \forall x > 0$, we interchange the summation and the integration and solve the integral, yielding

$$f(d_1, \gamma, l_a, l_b) = \sum_{k=0}^{\infty} \left(\frac{-1}{d_1^\eta \gamma} \right)^k \frac{x^{2+\eta k}}{\eta k + 2}.$$

Finally, we put the summation in the form of the Gauss Hypergeometric function ${}_2F_1(a, b; c; z)$ [27] and resort to the Pochhammer function, $(a)_k = a(a+1) \cdots (a+k-1) = \frac{\Gamma(a+k)}{\Gamma(a)}$, and to $\frac{(b)_k}{(b+1)_k} = \frac{b}{b+k}$, which yields the final form of $f(\cdot)$ as

$$\begin{aligned} f(d_1, \gamma, l_a, l_b) &= \frac{x^2}{2} \sum_{k=0}^{\infty} \frac{(1)_k}{k!} \frac{\left(\frac{2}{\eta}\right)_k}{\left(1 + \frac{2}{\eta}\right)_k} \left(-\frac{x^\eta}{d_1^\eta \gamma}\right)^k \\ &= \frac{x^2}{2} {}_2F_1\left(1, \frac{2}{\eta}; 1 + \frac{2}{\eta}; -\frac{x^\eta}{d_1^\eta \gamma}\right) \Big|_{l_b}^{l_a}. \quad (10) \end{aligned}$$

Now, as in [10], we consider interference from all SFs, *i.e.*,

$$\text{SIR} = \frac{|h_1|^2 g(d_1) \mathcal{P}_t}{\sum_{j \in \mathcal{S}} \mathcal{I}_j}. \quad (11)$$

Following an analysis similar to the case for one SF, we arrive in a combination of the received signals from all SFs weighted by the isolation thresholds Δ , where i denotes the SF ring of the desired node. Thus, the *capture probability* is

$$\begin{aligned} Q_1(d_1) &= \prod_{j \in \mathcal{S}} P_{\text{SIR}_j}(d_1, j) \\ &= \exp \left(-2\pi \sum_{j \in \mathcal{S}} \alpha_j f(d_1, \delta_{i,j}, l_{j-1}, l_j) \right). \quad (12) \end{aligned}$$

C. Outage Condition 3: External Interference

Orfanidis *et al.* [6] report the selectivity of LORA receivers in the presence of IEEE 802.15.4G signals. We use Orfanidis *et al.* experimentally obtained isolation thresholds to analyze the SIR in the presence of external interference generated by an IEEE 802.15.4G network. Here, we model the IEEE 802.15.4G network as PPP Φ_z and consider [6]

$$\Theta_{[dB]} = \begin{bmatrix} SF_7 & SF_8 & SF_9 & SF_{10} & SF_{11} & SF_{12} \\ -6 & -9 & -12.5 & -16 & -16 & -16 \end{bmatrix},$$

where Θ denotes the LORA vs. IEEE 802.15.4G SIR threshold vector, and θ_i denotes the i -th element of Θ , *i.e.*, the SIR threshold for the desired signal in SF ring i and interference from the IEEE 802.15.4G network.

The analysis of the LoRa capture probability in the presence of IEEE 802.15.4G interference is similar to the case for one SF (P_{SIR_j}), but taking the Θ vector and the IEEE 802.15.4G network parameters into account. For

$$\text{SIR}_z = \frac{|h_1|^2 g(d_1) \mathcal{P}_t}{\sum_{k \in \Phi_z} |h_k|^2 g(d_k) \mathcal{P}_t}, \quad (13)$$

the *capture probability* with respect to external interference is

$$Z_1(d_1) = P_{\text{SIR}_z}(d_1) = \exp(-2\pi\alpha_z f(d_1, \theta_i, 0, R_z)). \quad (14)$$

D. Coverage Probability

The *coverage probability* is the probability that the selected node is in coverage (not in outage), *i.e.*, it can successfully communicate considering all the outage conditions defined above. The coverage probability of the desired node is thus

$$C_1(d_1) = H_1(d_1) Q_1(d_1) Z_1(d_1). \quad (15)$$

V. OPTIMUM LORAWAN CONFIGURATION

The expressions in Section IV determine the expected reliability of a single node located at a given distance from the gateway. *However, what if one wants to plan the network deployment?* In this section, we consider the use of the previous model to this end. We first consider the inversion of the expressions in the model to obtain network configurations for a targeted minimum average reliability. Afterward, we propose two algorithms that derive optimum network configurations supporting the desired minimum reliability requirement.

A. Guaranteeing the Reliability Target

To start our search for optimal LORAWAN configurations we invert the previously described outage expressions defined in (5) and (12), so the network parameters can be extracted from them to achieve a minimum desired reliability level. Note that (14) does not depend on the LORAWAN configuration. It is, however, taken into account in the optimization algorithm proposed in Sections V-B and V-C to consider external interference. One can assume that, in our network model, the nodes presenting the worst average reliability in each SF ring are those on the ring outer limit. It happens because the signals emitted by those nodes suffer greater path-loss and are, therefore, more susceptible to interference.

1) *SF Ring Limits*: As a first step, we find the maximum distance that ensures the required minimum average reliability level w.r.t. the connection probability H_1 . We denote this threshold by \mathcal{T}_{H_1} . We rewrite (5) to perform operations over the SNR threshold ψ_i in Ψ and the outer SF ring limit l_i ,

$$\mathcal{T}_{H_1} = \exp\left(-\frac{\mathcal{N}\psi_i}{\mathcal{P}_t g(l_i)}\right), \quad (16)$$

and then it is straightforward to obtain

$$l_i = \frac{\lambda}{4\pi} \left[-\frac{\mathcal{P}_t \ln(\mathcal{T}_{H_1})}{\mathcal{N}\psi_i}\right]^{\frac{1}{\eta}}. \quad (17)$$

Note that the radius of the overall coverage area is $R = l_6$.

2) *Ring Densities*: Since (17) defines the network geometry, it is now possible to obtain the outage due to external interference observed by the nodes at each ring edge from $Z_1(l_i)$. After that, we compute the maximum densities of the PPPs in Q_1 that satisfy the given final reliability target \mathcal{T} , the previously assumed connection reliability target \mathcal{T}_{H_1} , and the external interference of each SF i . Thus, following (15), making $C_1(l_i) = \mathcal{T}$ and $H_1(l_i) = \mathcal{T}_{H_1}$, we have for each SF ring i that $\mathcal{T} = \mathcal{T}_{H_1} Q_1(l_i) Z_1(l_i)$, and thus

$$\frac{\mathcal{T}}{\mathcal{T}_{H_1} Z_1(l_i)} = \exp\left(-2\pi \sum_{j \in S} \alpha_j f(l_i, \delta_{i,j}, l_{j-1}, l_j)\right). \quad (18)$$

In (18), the function $f(\cdot)$ is independent of α_j if the SF limits are pre-defined. Then, let $y_{i,j} = f(l_i, \delta_{i,j}, l_{j-1}, l_j)$ and $b_i = -\frac{1}{2\pi} \ln\left(\frac{\mathcal{T}}{\mathcal{T}_{H_1} Z_1(l_i)}\right)$, yielding, for each SF ring i ,

$$y_{i,1}\alpha_1 + y_{i,2}\alpha_2 + y_{i,3}\alpha_3 + y_{i,4}\alpha_4 + y_{i,5}\alpha_5 + y_{i,6}\alpha_6 = b_i. \quad (19)$$

If we name the vectors $A = [\alpha_1, \dots, \alpha_6]$, $B = [b_1, \dots, b_6]$, and the matrix $Y = [y_{i,j}]$, $\forall i, j \in S$, from (19) we derive a system of linear equations $Y \times A = B$ and solve it for the PPPs densities A by making

$$A = Y^{-1} \times B. \quad (20)$$

Note that Y is a $|S| \times |S|$ square matrix, both A and B are row vectors of length $|S|$, and all values $y_{i,j}$ in Y are positive real numbers. Considering the diagonal method to compute the determinant of Y , it is possible to observe that, due to Δ , the values at $i = j$ are significantly higher than when $i \neq j$, thus making the positive diagonal greater than the negative diagonal, incurring in a determinant that is virtually never zero.

B. Maximization of Communication Range

The expressions presented above allow us to obtain twelve network parameters: six communication range limits $L = [l_1, \dots, l_6]$ from (17), and six PPP densities $A = [\alpha_1, \dots, \alpha_6]$ from (20). Note that (20) depends on (17) because of L . Combining both equations generates an incomplete linear system of six equations and twelve variables. In order to search for optimized feasible network configurations, we propose an algorithm that uses (17) and (20) in an iterative method,

trying to extend the SF ring outer limits as much as possible, while preserving the targeted final reliability level \mathcal{T} and ensuring service to a minimum quantity of nodes (N_{min}). The algorithm extends the SF ring outer limits by reducing \mathcal{T}_{H_1} . Similarly, increasing \mathcal{T}_{H_1} shortens these limits. The algorithm, iteratively guesses values for \mathcal{T}_{H_1} and then, after obtaining L through (17), analyzes the maximum possible densities A . As \mathcal{T}_{H_1} gets closer to \mathcal{T} , the capture probability Q_1 increases and, with fixed L and Z_1 , higher Q_1 is possible only with lower densities. It may lead to configurations breaking the N_{min} restriction. Conversely, if \mathcal{T}_{H_1} is too close to 1, the outer limits of the SF rings will be shorter, leading to small coverage areas that are useless in practice. However, the proposed algorithm identifies feasible ranges for the network parameters, thus dealing with this parameter trade-off.

Algorithm 1 employs a branch-and-bound technique to explore the network design space (*i.e.*, possible values of \mathcal{T}_{H_1}), seeking to maximize the width of each SF ring and, as a consequence, the network communication range (disk radius), while preserving the targeted minimum reliability \mathcal{T} and ensuring service to, at least, a given number of nodes (N_{min}). The branch-and-bound technique fits well to our problem because it reduces the design space in half in each iteration, accelerating convergence. The inputs of the algorithm are the targeted reliability \mathcal{T} , the duty-cycle vector p , N_{min} , and the density of IEEE 802.15.4G interfering nodes α_z . The algorithm outputs a *result* variable stating if the algorithm converged (1) or not (-1), the achieved number of nodes N , and the vectors L and A containing, respectively, the SF limits and ring densities that ensure the desired reliability.

After initializing the variables (lines 1-4), the optimization loop starts and runs until the algorithm converges (line 26) or diverges (line 23). The optimization procedure “guesses” values for \mathcal{T}_{H_1} , trying to reduce it to enlarge the width of each SF ring, thus increasing the coverage area. Note that since C_1 depends on H_1 from (15), \mathcal{T}_{H_1} must be greater than \mathcal{T} ; otherwise, both Q_1 and Z_1 would have to be 1, what is impossible in practice. Thus, Algorithm 1 sets the initial search region for \mathcal{T}_{H_1} to $(\mathcal{T}, 1)$. The guessed value for \mathcal{T}_{H_1} in each iteration is at the center of this region, as expressed in line 6. At each iteration, if the selected \mathcal{T}_{H_1} generates a configuration where the number of nodes is above N_{min} , it is assumed that Q_1 can be enhanced by decreasing N , what allows for further decreasing \mathcal{T}_{H_1} in the next iteration. Conversely, if $N < N_{min}$, \mathcal{T}_{H_1} is increased so that Q_1 can be lower, allowing for more nodes in the network. This “binding” part of the algorithm is in lines 30-34.

Provided the branch-and-bound technique guesses \mathcal{T}_{H_1} in line 6, the range limits for all SF are computed using (17) in line 7. In the following, the algorithm uses the newly computed vector L to obtain vector B and matrix Y (lines 11-16), allowing for the computation of the PPPs densities in A (line 17), using (20). Following that, the number of nodes fitting the generated configuration is computed by first obtaining the area of each SF ring in lines 18-19 as $V_i = \pi(l_i^2 - l_{i-1}^2)$. The algorithm converges and stops when the difference in the radius R of the overall coverage area between two consecutive iterations is less than χ (line 20) and $N > N_{min}$ (line 21),

Algorithm 1 Maximization of SF rings widths given the target reliability (\mathcal{T}) and the minimum number of nodes (N_{min}).

Input: $\mathcal{T}, p, N_{min}, \alpha_z$

Output: result, A, L, N

```

1:  $\mathcal{T}_{H_1, max} \leftarrow 1$ 
2:  $\mathcal{T}_{H_1, min} \leftarrow \mathcal{T}$ 
3:  $R \leftarrow 0, N \leftarrow 0$ 
4: result  $\leftarrow 0$ 
5: while result = 0 do
6:    $\mathcal{T}_{H_1} \leftarrow (\mathcal{T}_{H_1, max} + \mathcal{T}_{H_1, min})/2$ 
7:    $L \leftarrow \frac{\lambda}{4\pi} \left[ -\frac{\mathcal{P}_t \ln(\mathcal{T}_{H_1})}{N\psi} \right]^{\frac{1}{\eta}}$  {Equation (17)}
8:    $R_{last} \leftarrow R$ 
9:    $R \leftarrow L[end]$ 
10:   $R_z \leftarrow R$ 
11:  for  $i = [1, \dots, 6]$  do
12:    for  $j = [1, \dots, 6]$  do
13:       $Y[i, j] \leftarrow f(l_i, \delta_{i,j}, l_j, l_{j+1})$ 
14:    end for
15:     $B[i] \leftarrow -\frac{1}{2\pi} \ln \frac{\mathcal{T}}{Z_1(l_i)\mathcal{T}_{H_1}}$ 
16:  end for
17:   $A \leftarrow Y^{-1} \times B$  {Equation (20)}
18:   $V \leftarrow \text{ComputeRingAreas}(L)$ 
19:   $N \leftarrow (Ap) \times V'$ 
20:  if  $\text{abs}(R - R_{last}) < \chi$  and  $A_i \geq 0, \forall A_i$  then
21:    if  $N < N_{min}$  then
22:      if  $\mathcal{T}_{H_1, max} - \mathcal{T}_{H_1, min} < \epsilon$  then
23:        result  $\leftarrow -1$ 
24:      end if
25:    else
26:      result  $\leftarrow 1$ 
27:    end if
28:  end if
29:  if result = 0 then
30:    if  $A_i \geq 0, \forall A_i$  and  $N \geq N_{min}$  then
31:       $\mathcal{T}_{H_1, max} = \mathcal{T}_{H_1}$ 
32:    else
33:       $\mathcal{T}_{H_1, min} = \mathcal{T}_{H_1}$ 
34:    end if
35:  end if
36: end while
37: return result,  $A, L, N$ 

```

where χ defines the precision of R . If the variation of R , i.e., $\text{abs}(R - R_{last})$, is too small and the algorithm did not achieve N_{min} yet, the algorithm keeps trying to converge until the variation in the guessed \mathcal{T}_{H_1} is below a threshold ϵ (line 22), in which case the algorithm stops and announces a divergence. After evaluating the proposed algorithm for a set of test scenarios, we concluded that good values for the stopping thresholds are $\chi = 1m$ and $\epsilon = 10^{-9}$.

Algorithm 1 always converges if there are feasible solutions to the problem. If the requirements of minimum network density (N_{min} and p), targeted reliability (\mathcal{T}), or both, are too high, however, the algorithm may take too long to converge. Hence, we stop the algorithm when the changes in \mathcal{T}_{H_1} get too small (line 22). Note that this guarantees the algorithm

to stop because $\mathcal{T}_{H_1, max} - \mathcal{T}_{H_1, min}$ decreases every iteration. It is important to note, however, that achieving higher network density is always possible by reducing the reliability requirement \mathcal{T} . Moreover, highly demanding scenarios without feasible solutions or with lengthy convergence are not typical in LORAWAN, since the technology has been conceived to support massive rather than critical IoT applications.

C. Maximization of Number of Nodes

In this section, we consider the case of maximizing the total number of nodes, given restrictions of minimum coverage radius (R_{min}) and average reliability (\mathcal{T}). In order to do that, we use a more straightforward approach than in Algorithm 1. The problem of maximizing the number of nodes is equivalent to the problem of minimizing Q_1 . Thus it is straightforward to conclude, from (15), that we should maximize H_1 because higher H_1 allows for lower Q_1 . Since we assume that the worst cases are at the edge of the SFs and we have a restriction on the coverage radius, the maximum possible H_1 is that yielding $l_6 = R_{min}$. Thus, from (5), we conclude that $\mathcal{T}_{H_1} = H_1(R_{min})$. Assuming the same \mathcal{T}_{H_1} for all SFs, we use (17) to compute L and obtain the geometry of the network.

Once we have obtained L , we get the maximum allowable densities ensuring \mathcal{T} through (20). Algorithm 2 shows the proposed procedure. Line 1 uses (5) to compute the maximum \mathcal{T}_{H_1} satisfying R_{min} . Line 2 uses the computed \mathcal{T}_{H_1} to obtain the geometry of the network L . The loop in lines 5-10 computes matrix Y and vector B , so the maximum device density vector A can be computed in line 11. Finally, after computing the areas of the rings and storing them in vector V (line 12), we obtain the maximum number of nodes in line 13.

Note that Algorithm 2 is not iterative since there is no loop searching for the optimum solution. It merely describes how to use the proposed models to determine the optimum LORAWAN configuration considering the restrictions. The approach produces unfeasible configurations if the restrictions are too strict. Thus, lines 14-18 check whether the method generated non-negative densities for all SFs in order to assess whether the results are feasible or not.

VI. NUMERICAL RESULTS

This section evaluates the proposed model and algorithms. In the figures, lines represent theoretical probabilities while marks are the average of Monte Carlo simulations with 10^5 random scenarios. Results consider the expressions for success probabilities H_1 , Q_1 , Z_1 , and C_1 as defined by (5), (12), (14), and (15), respectively. Moreover, we assume $F = 6$ dB, $\eta = 2.75$, $\lambda = c/f$ m, $c = 3 \times 10^8$ m/s (speed of light), $f = 868$ MHz for both LORAWAN and IEEE 802.15.4G. LORAWAN channel bandwidth is $B_l = 125$ kHz, and IEEE 802.15.4G channel bandwidth is $B_z = 200$ kHz. We also assume that nodes in LORAWAN and IEEE 802.15.4G transmit with $\mathcal{P}_t = 14$ dBm. These parameters configure typical sub-urban scenarios following European regulations.

Concerning IEEE 802.15.4G interference, we evaluate the algorithms considering three scenarios. In real deployments,

Algorithm 2 Maximization of the number of nodes given the target reliability (\mathcal{T}) and the minimum coverage radius (R_{min}).

Input: $\mathcal{T}, p, R_{min}, \alpha_z$

Output: result, A, L, N_{max}

- 1: $\mathcal{T}_{H_1} \leftarrow \exp\left(-\frac{N\psi_6}{\mathcal{P}_t g(R_{min})}\right)$ {Equation (5)}
- 2: $L \leftarrow \frac{\lambda}{4\pi} \left[-\frac{\mathcal{P}_t \ln(\mathcal{T}_{H_1})}{N\psi}\right]^{\frac{1}{\eta}}$ {Equation (17)}
- 3: $R \leftarrow L[end]$
- 4: $R_z \leftarrow R$
- 5: **for** $i = [1, \dots, 6]$ **do**
- 6: **for** $j = [1, \dots, 6]$ **do**
- 7: $Y[i, j] \leftarrow f(l_i, \delta_{i,j}, l_j, l_{j+1})$
- 8: **end for**
- 9: $B[i] \leftarrow -\frac{1}{2\pi} \ln \frac{\mathcal{T}}{Z_1(l_i)\mathcal{T}_{H_1}}$
- 10: **end for**
- 11: $A \leftarrow Y^{-1} \times B$ {Equation (20)}
- 12: $V \leftarrow \text{ComputeRingAreas}(L)$
- 13: $N_{max} \leftarrow (Ap) \times V'$
- 14: **if** $A_i \geq 0, \forall A_i$ **then**
- 15: result $\leftarrow 1$
- 16: **else**
- 17: result $\leftarrow -1$
- 18: **end if**
- 19: **return** result, A, L, N_{max}

the designer of a LORAWAN network may not know the operational parameters of the interfering IEEE 802.15.4G network. Thus, in a practical situation, the designer should assume worst-case configurations for the external network.

A. Model Validation

Figure 2 aims to validate the presented models by showing the success rates H_1 , Q_1 , Z_1 , and C_1 as a function of the distance from the gateway. The scenario considers an average number of nodes $\bar{N} = 4000$, transmitting with duty cycle $p = 0.1\%$ in a circular area around the gateway with radius $R = 4000\text{m}$. The IEEE 802.15.4G network generating external interference has $\bar{N}_z = 1000$ nodes transmitting with duty cycle $p_z = 0.1\%$, also in a circular area with radius $R_z = 4000\text{m}$. As can be seen, all theoretical expressions (lines) match the simulation results (marks). One can observe in Z_1 that a relatively light interference from IEEE 802.15.4G ($\bar{N}_z = 1000, p_z = 0.1\%$) has little impact in lower SFs due to the smaller ToA and reduced probability of concurrent transmissions. Higher SFs, on the other hand, have higher ToA and thus suffer more from this external interference.

Also in Figure 2, Q_1^* shows what the capture probability would be if we consider that LORA signals are perfectly orthogonal. We obtain Q_1^* from (12) by considering only $j = i$. As can be seen, the gap between Q_1 and Q_1^* shows that inter-SF interference plays an important role in link quality.

B. Algorithm 1: Maximization of R

Now we evaluate Algorithm 1 of Section V-B. These results use the same network parameters employed to validate the

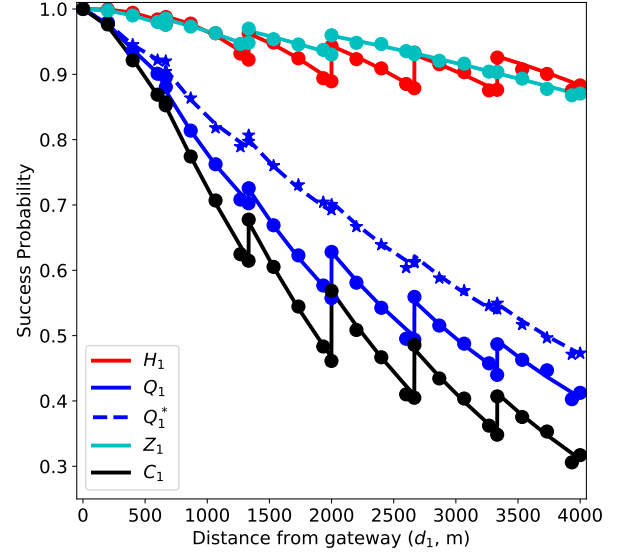


Figure 2. Success probabilities of all outage sources. LORA: $\bar{N} = 4000, p = 0.1\%, \eta = 2.75, \mathcal{P}_t = 14\text{dBm}, R = 4000\text{m}$. IEEE 802.15.4G: $\bar{N}_z = 1000, p_z = 0.1\%, \eta = 2.75, \mathcal{P}_t = 14\text{dBm}, R_z = 4000\text{m}$.

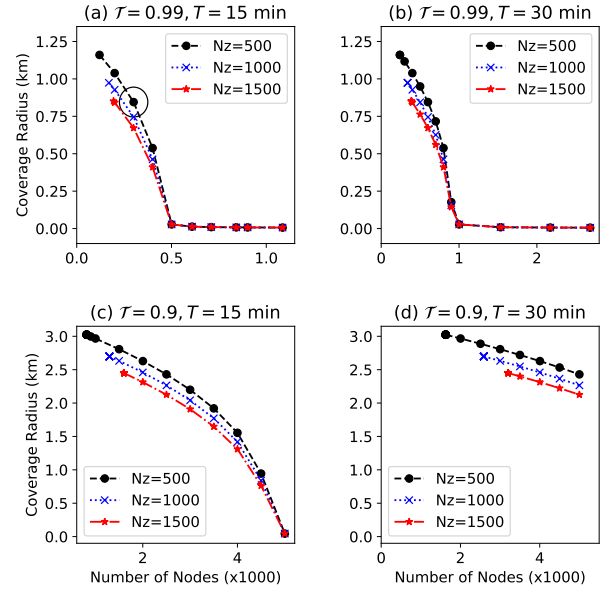


Figure 3. Optimization between coverage and number of nodes given a minimum reliability constraint when maximizing R with Algorithm 1.

network model. Figure 3 presents a series of graphs for varying optimization objectives. Plots in the same row consider the same reliability target \mathcal{T} , while plots in the same column use the same packet generation interval T , expressed in minutes. Each graph shows three curves, each one considering a different amount of IEEE 802.15.4G interference, which varies by changing the number of IEEE 802.15.4G nodes (\bar{N}_z), always with duty cycle $p_z = 0.1\%$. Each optimization point considers different N_{min} values, evaluated for every 100m.

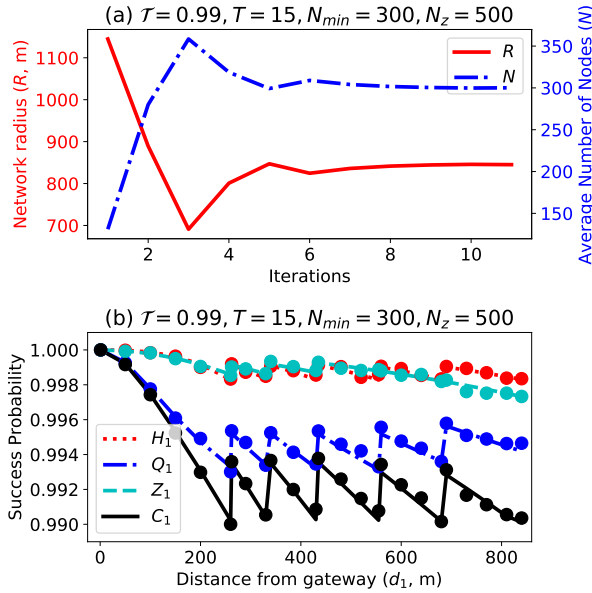


Figure 4. Convergence of Algorithm 1 and success probability for the scenario marked in Figure 3-a.

The first conclusion when comparing the curves in all plots is that different IEEE 802.15.4G interference leads to shorter communication ranges when following our proposed optimization procedure. That makes sense since shorter distances feature smaller path loss, making signals less susceptible to external interference. It is also possible to observe that less stringent reliability targets lead to larger coverage areas. Again, that makes sense since smaller \mathcal{T} yields smaller \mathcal{T}_{H_1} , which in turn enables longer communication range.

Also in Figure 3, plot (a) shows the more rigorous scenario; the configuration allowing the required reliability is only practical for $N_{min} \leq 400$ nodes, with a radius varying from 410 to 1160 meters, depending on N_{min} and the external interference. The coverage radius with $N_{min} \geq 500$ either converged to unpractical distances of less than 10 meters or diverged, meaning that it was not possible to place such a number of LORAWAN nodes with packet generation interval of 15 minutes while ensuring minimum reliability of $\mathcal{T} = 0.99$.

For $\mathcal{T} = 0.99$, more feasible and useful scenarios exist if one reduces network usage. Plot 3-(b) shows that configurations with up to 900 nodes are possible if the packet transmission interval is $T = 30$ minutes. For $\mathcal{T} = 0.9$ with $T = 15$ minutes, it is possible to find reasonably good network configurations up to $N_{min} = 4500$. However, $N_{min} = 5000$ shrinks the communication range to unpractical distances.

Figure 4 illustrates the behavior of Algorithm 1 and the network performance when taking the circled case in Figure 3-(a) as an example. Figure 4-(a) shows the convergence of R and \bar{N} for this scenario. We see that $\bar{N} = 300.1$ in the last iteration converges to N_{min} , thus “stretching” the network range as much as possible.

Table II shows numerical results of the same scenario in two columns: “All sources”, with the results for our com-

Table II. DETAILED OPTIMIZATION RESULTS FOR THE MARKED SCENARIO IN FIGURE 3-A.

Interference:		All sources			Intra-SF only		
Scenario	SF	Range (m)	\bar{N}_i	\bar{N}	Range (m)	\bar{N}_i	\bar{N}
3-(a)	7	261.6	162.8	300.1	370.0	124.6	300.03
	8	336.4	67.5		475.7	87.1	
	9	432.4	32.5		611.6	43.5	
	10	555.9	21.8		786.2	25.3	
	11	685.4	10.6		969.3	12.9	
	12	845.0	4.7		1195.1	6.4	

plete model, and “Intra-SF only”, disregarding both inter-SF and external interference sources. We get the results in the “Intra-SF only” column using the same models, but setting $\theta_i = -\infty, \forall i \in S$ in Θ , and $\delta_{i,j} = 1$ for $i = j$ and $\delta_{i,j} = -\infty$ otherwise. When considering all sources of interference, as expected, the fact that ToA impacts the duty cycle induces the optimization procedure to allocate most of the nodes with lower SF. That happens because signal attenuation increases with distance, making more distant nodes more vulnerable to both internal and external interference. Recall that a shorter ToA reduces the collision probability. Moreover, longer ToA generates more internal interference to other SFs. In some cases, higher SFs may not be used to ensure minimum reliability. However, note that (17), (20) and Algorithm 1 can be extended to change the restriction N_{min} to represent a vector with the minimum number of nodes using each SF. One can achieve that by revisiting the computation of the densities in (20) to consider such a minimum number of nodes when computing the spatial density. Since doing that will possibly result in more nodes using higher SFs, it is expected that fewer nodes use lower SF, resulting in a smaller total number of nodes, as well as a shorter network radius, since the algorithm will converge to a higher H_1 to compensate the increased Q_1 . When disregarding inter-SF and external interference, we observe that higher SFs are highly affected by inter-SF and external interference, especially due to their extended ToA. In particular, we observe that interference, rather than path loss, is the main factor for which our method disfavors the use of higher SF. Moreover, it is clear that interference considerably affects coverage.

Finally, Figure 4-(b) shows the success probabilities of the example scenario, where the optimized configurations are w.r.t. the minimum average reliability target \mathcal{T} for all distances from the gateway. As expected, the success probability approaches the desired minimum $\mathcal{T} = 0.99$ at the edge of each SF. We can see that collisions (Q_1) are kept almost constant or increase slightly with SF. That happens because the algorithm reduces the number of nodes using each SF to keep Q_1 in pace with H_1 and Z_1 , to ensure the minimum \mathcal{T} .

C. Algorithm 2: Maximization of \bar{N}

Now we evaluate Algorithm 2 of Section V-C. The plots in Figure 5 show the results for different scenarios of required minimum reliability (\mathcal{T}) and message generation period (T). For all plots, the x-axis represents the R_{min} input to the

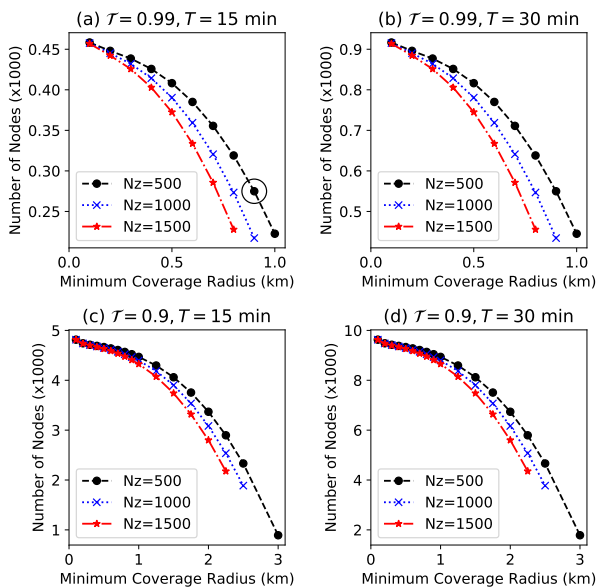


Figure 5. Optimization between the number of nodes and coverage given a minimum reliability constraint when maximizing \bar{N} with Algorithm 2.

Table III. DETAILED OPTIMIZATION RESULTS FOR THE MARKED SCENARIO IN FIGURE 5-A.

Scenario	SF	All sources			Intra-SF only		
		Range (m)	\bar{N}_i	\bar{N}	Range (m)	\bar{N}_i	\bar{N}
5-(a)	7	278.7	149.2	274.9	278.7	211.1	508.2
	8	358.3	61.8		358.3	147.6	
	9	460.6	29.9		460.6	73.7	
	10	592.1	20.2		592.1	42.9	
	11	730.0	9.5		730.0	21.8	
	12	900.0	4.0		900.0	10.9	

algorithm, while the y-axis shows the achieved maximized number of nodes. In each plot, the x-axis grows up to the value for which the requirements yield practical results.

In Figure 5, if we analyze each row of plots independently, we see that the maximum number of nodes is a linear function of the transmission period T . For instance, considering $R_{min} = 500\text{m}$ and $N_z = 500$, N_{max} in plots 5-(a) and 5-(b) are, respectively, 408.18 and 816.36, *i.e.*, N_{max} doubles when T doubles. That is expected since these variations ensure the same network load in all scenarios. We can also observe that, in all plots, increased external interference reduces both the number of supported nodes and the achievable coverage radius.

Table III shows the achieved geometry and number of nodes of the marked scenario of Figure 5-(a). Again, the ‘‘All sources’’ column presents the results of our complete model, while the ‘‘Intra-SF only’’ column disregards inter-SF and external interference. Since the method assumes that the maximum number of nodes is achieved with the shortest possible distances, the maximum range of a node using SF₁₂ has to be R_{min} (900m for this case). As for Algorithm 1, Algorithm 2 also favors lower SFs. Moreover, Table III shows that the maximum number of nodes almost doubles when

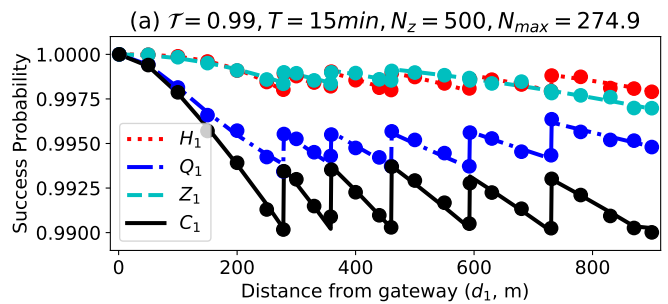


Figure 6. Average outage expectation for the marked scenario in Figure 5.

disregarding inter-SF and external interference, emphasizing the importance of taking such impairments into account to avoid overestimating the network performance. Finally, Figure 6 shows the success probabilities for the example scenario, which approach $\mathcal{T} = 0.99$ at the SF edges, but stay above the required minimum \mathcal{T} for all distances smaller than R_{min} .

VII. CONCLUSION

This paper presents two algorithms to optimize the configuration of LORAWAN under imperfect SF orthogonality and IEEE 802.15.4G interference. We use models of LORAWAN networks to derive success probabilities of packet delivery under internal and external (IEEE 802.15.4G) interference. The presented algorithms search for optimum LORAWAN configurations given restrictions of minimum network density or coverage radius, meeting a target minimum reliability level. The analytic results are validated using simulations.

Regarding IEEE 802.15.4G interference over LORAWAN, although higher SF should be more robust to this type of interference, they tend to suffer more from that impairment because their increased ToA makes it more likely that transmissions overlap with IEEE 802.15.4G activity. Finally, regarding the proposed algorithms, they can provide a tool for exploring trade-offs between network load and coverage range by showing the feasible region of LORAWAN network configurations.

REFERENCES

- [1] M. Centenaro, L. Vangelista, A. Zanella, and M. Zorzi, ‘‘Long-range communications in unlicensed bands: the rising stars in the IoT and smart city scenarios,’’ *IEEE Wireless Communications*, vol. 23, no. 5, pp. 60–67, Oct 2016.
- [2] C. Bockelmann, N. Pratas, H. Nikopour, K. Au, T. Svensson, C. Stefanovic, P. Popovski, and A. Dekorsy, ‘‘Massive machine-type communications in 5G: physical and mac-layer solutions,’’ *IEEE Communications Magazine*, vol. 54, no. 9, pp. 59–65, Sep 2016.
- [3] LoRa Alliance. (2019, Mar) Website. [Online]. Available: <http://www.lora-alliance.org>
- [4] Wi-SUN Alliance. (2019, Mar) Website. [Online]. Available: <http://www.wi-sun.org>
- [5] K.-H. Chang and R. Mason, ‘‘The ieee 802.15.4g standard for smart metering utility networks,’’ in *2012 IEEE Third International Conference on Smart Grid Communications*, Nov 2012, pp. 476–480.
- [6] C. Orfanidis, L. M. Feeney, M. Jacobsson, and P. Gunningberg, ‘‘Investigating interference between lora and ieee 802.15.4g networks,’’ in *IEEE 13th International Conference on Wireless and Mobile Computing, Networking and Communications*, Oct 2017, pp. 1–8.

- [7] L. Krupka, L. Vojtech, and M. Neruda, "The issue of lpwan technology coexistence in iot environment," in *2016 17th International Conference on Mechatronics - Mechatronika*, Dec 2016.
- [8] E. D. Poorter, J. Hoebeke, M. Strobbe, I. Moerman, S. Latré, M. Weyn, B. Lannoo, and J. Famaey, "Sub-ghz lpwan network coexistence, management and virtualization: An overview and open research challenges," *Wireless Personal Communications*, vol. 95, no. 1, pp. 187–213, Jul 2017.
- [9] A. Hoeller-Jr., R. D. Souza, O. L. A. López, H. Alves, M. de Noronha-Neto, and G. Brante, "Analysis and performance optimization of lora networks with time and antenna diversity," *IEEE Access*, vol. 6, pp. 32 820–32 829, Jul 2018.
- [10] A. Mahmood, E. G. Sisinni, L. Guntupalli, R. Rondón, S. A. Hassan, and M. Gidlund, "Scalability analysis of a lora network under imperfect orthogonality," *IEEE Transactions on Industrial Informatics*, vol. 15, no. 3, pp. 1425–1436, March 2019.
- [11] O. Georgiou and U. Raza, "Low power wide area network analysis: Can lora scale?" *IEEE Wireless Communications Letters*, vol. 6, no. 2, pp. 162–165, Apr 2017.
- [12] D. Croce, M. Gucciardo, S. Mangione, G. Santaromita, and I. Tinnirello, "Impact of lora imperfect orthogonality: Analysis of link-level performance," *IEEE Communications Letters*, vol. 22, no. 4, pp. 796–799, Apr 2018.
- [13] R. B. Sørensen, D. M. Kim, J. J. Nielsen, and P. Popovski, "Analysis of latency and mac-layer performance for class a lorawan," *IEEE Wireless Communications Letters*, vol. 6, no. 5, pp. 566–569, Oct 2017.
- [14] A.-I. Pop, U. Raza, P. Kulkarni, and M. Sooriyabandara, "Does bidirectional traffic do more harm than good in lorawan based lpwa networks?" in *2017 IEEE Global Communications Conference*, Dec 2017, pp. 1–6.
- [15] N. Abramson, "The ALOHA system - another alternative for computer communications," in *Fall Joint Computer Conference*, Dec 1970, pp. 281–285.
- [16] *AN120.22 LoRa Modulation Basics*, Semtech Corporation, Mar 2015.
- [17] *SX1272/73 - 860 MHz to 1020 MHz Low Power Long Range Transceiver*, Semtech Corporation, Mar 2017.
- [18] IEEE Std 802.15.4g-2012 (Amendment to IEEE Std 802.15.4-2011), "IEEE standard for local and metropolitan area networks - part 15.4: Low-rate wireless personal area networks (lr-wpans) amendment 3: Physical layer (phy) specifications for low-data-rate, wireless, smart metering utility networks," Apr 2012.
- [19] H. Harada, K. Mizutani, J. Fujiwara, K. Mochizuki, K. Obata, and R. Okumura, "Ieee 802.15.4g based wi-sun communication systems," *IEICE Transactions on Communications*, vol. E100.B, no. 7, pp. 1032–1043, 2017.
- [20] M. K. Oh, J. Y. Kim, S. Lee, Y. Jeon, and S. Choi, "A fully integrated IEEE 802.15.4g MR-FSK SoC for smart utility network applications," *IEEE Transactions on Consumer Electronics*, vol. 60, no. 4, pp. 580–586, Nov 2014.
- [21] J. Muñoz, T. Chang, X. Vilajosana, and T. Watteyne, "Evaluation of ieee802.15.4g for environmental observations," *Sensors (Basel)*, vol. 18, no. 10, 2018.
- [22] IEEE Std 802.15.4e-2012 (Amendment to IEEE Std 802.15.4-2011), "IEEE standard for local and metropolitan area networks - part 15.4: Low-rate wireless personal area networks (lr-wpans) amendment 1: Mac sublayer," Apr 2012.
- [23] U. Deshpande, D. Kotz, and C. McDonald, "Coordinated sampling to improve the efficiency of wireless network monitoring," in *15th IEEE International Conference on Networks*, Nov 2007, pp. 353–358.
- [24] M. Haenggi and R. K. Ganti, "Interference in large wireless networks," *Foundations and Trends in Networking*, vol. 3, no. 2, pp. 127–248, Nov 2009.
- [25] A. Goldsmith, *Wireless Communications*. USA: Cambridge University Press, 2005.
- [26] C. Goursaud and J.-M. Gorce, "Dedicated networks for IoT: PHY/MAC state of the art and challenges," *EAI Endorsed Transactions on Internet of Things*, vol. 15, no. 1, pp. 1–11, Oct 2015.
- [27] A. B. O. Daalhuis, "Hypergeometric function," in *NIST Handbook of Mathematical Functions*, 1st ed., F. W. J. Olver, D. W. Lozier, R. F. Boisvert, and C. W. Clark, Eds. New York, USA: Cambridge University Press, 2010, ch. 15, pp. 383–402.